A Versatile Family of Interconvertible Microporous Chiral Molecular Frameworks: The First Example of Ligand Control of Network Chirality

C. J. Kepert,† T. J. Prior, and M. J. Rosseinsky*

Contribution from the Department of Chemistry, University of Liverpool, Liverpool L69 7ZD, United Kingdom, and School of Chemistry, University of Sydney, NSW 2006, Australia

Received October 26, 1999. Revised Manuscript Received February 1, 2000

Abstract: Two families of molecular frameworks which grow as homochiral single crystals are described. Both consist of multiple interpenetration of the three-connected chiral (10,3)-a (Y*) network and result from the tridentate coordination of the 1,3,5-benzenetricarboxylate (btc) ligand to octahedral metal centers which act as linear connectors. The nature of the interpenetration is controlled by the auxiliary ligands bound in the equatorial plane of the metal center. Ethylene glycol (eg) binds in a unidentate fashion to form phase **A** which has 28% accessible solvent volume and contains four interpenetrating (10,3)-a networks. 1,2-Propanediol (1,2-pd) coordinates as a bidentate ligand to yield a phase **B** with a greatly enhanced 51% of solvent accessible volume, because only two (distorted) (10,3)-a′ networks interpenetrate. Ligands in the void space and bound to the metal center can both be liberated thermally: the kinetics of this process allow isolation of microporous desolvated crystalline **A** and **B**. The porous phases lose crystallinity reversibly upon further loss of ligands bound to the equatorial metal: crystallinity is restored upon exposure to the vapors of simple alcohols, which can also effect conversion of **B** to **A**. Both phases present interpenetrating network topologies that are unique to chemistry and adopt space groups that are new for molecular solids: **A** crystallizes in $P4_232$ and **B** adopts $I4_132$. **B** can be grown homochirally from enantiomerically pure diol template. The stereochemistry of the alcohol bound to the metal controls the helicity of the chiral framework. The structure determination of the 1,2-propanediol phase represents the first demonstration that chiral molecules can specifically template helix handedness in a chiral porous framework solid.

Introduction

Molecular framework solids formed by inorganic coordination polymer networks[1] are currently attracting considerable attention in view of possible applications in selective sorption and catalysis.[2] Frameworks which are robust to guest exchange,[3] are microporous,[4] and display zeolite-like structural stability to guest removal[5] are now known. The extent to which the network structure and chemical nature of the pores can be manipulated to prepare porous solids with structures and sorptive/exchange properties different from those of the well-known zeolite and ALPO framework hosts is as yet uncertain.

One area in which traditional frameworks have not made considerable impact is enantioselective sorption and catalysis due to the difficulty in preparing such phases in chiral structures without enantiomer intergrowth within single crystallites and with void volume accessible either by template removal or exchange.[6] Chiral functionalization of achiral zeolitic frameworks has been demonstrated.[7] The aluminosilicate zeolite β[8] and the titanosilicate ETS-10[9] are multiphasic and retain enantiopurity only over a few crystallographic layers. Single-crystal growth has allowed resolution of chiral zincophos-

* Address correspondence to this author at the University of Liverpool. Phone: 44 (0)151 794 3499. Fax: 44 (0)151 794 3587. E-mail: m.j.rosseinsky@liv.ac.uk.

† University of Sydney.

(1) (a) Hoskins, B. F.; Robson, R. *J. Am. Chem. Soc.* **1990**, *112*, 1546. (b) Batten, S. R.; Robson, R. *Angew. Chem., Int. Ed. Engl.* **1998**, *37*, 1461. (c) Blake, A. J.; Champness, N. R.; Hubberstey, P.; Li, W.-S.; Withersby, M. A.; Schröder, M. *Coord. Chem. Rev.* **1999**, *183*, 117−138. (d) Choi, H. J.; Suh, M. P. *J. Am. Chem. Soc.* **1998**, *120*, 10628.

(2) (a) Barton, J. B.; Bull, L. M.; Klemperer, W. G.; Loy, D. A.; McEnaney, B.; Misono, M.; Monson, P. A.; Pez, G.; Scherer, G. W.; Vartuli, J. C.; Yaghi, O. M. *Chem. Mater.* **1999**, *11*, 2633−2656. (b) Yaghi, O. M.; Li, H. L.; Davis, C.; Richardson, D.; Groy, T. L. *Acc. Chem. Res.* **1998**, *31*, 474. (c) Yaghi, O. M.; Li, G. M.; Li, H. L. *Nature* **1995**, *378*, 703−706. (d) Fujita, M.; Kwon, Y. J.; Washizu, S.; Ogura, K. *J. Am. Chem. Soc.* **1994**, *116*, 1151−1152.

(3) (a) Chui, S. S. Y.; Lo, S. M. F.; Charmant, J. P. H.; Orpen, A. G.; Williams, I. D. *Science* **1999**, *283*, 1148−1150. (b) Kondo, M.; Yoshitomi, T.; Seki, K.; Matsuzaka, H.; Kitagawa, S. *Angew. Chem., Int. Ed. Engl.* **1997**, *36*, 1725−1727.

(4) (a) Reineke, T. M.; Eddaoudi, M.; O'Keeffe, M.; Yaghi, O. M. *Angew. Chem., Int. Ed. Engl.* **1999**, *38*, 2590−2594. (b) Li, H.; Eddaoudi, M.; Groy, T. L.; Yaghi, O. M. *J. Am. Chem. Soc.* **1998**, *120*, 8571−8572. (c) Kondo, M.; Okubo, T.; Asami, A.; Noro, S.; Yoshitomi, T.; Kitagawa, S.; Ishii, T.; Matsuzaka, H.; Seki, K. *Angew. Chem., Int. Ed. Engl.* **1999**, *38*, 140−143. (d) Eddaoudi, M.; Li, H. L.; Reineke, T.; Fehr, M.; Kelley, D.; Groy, T. L.; Yaghi, O. M. *Top. Catal.* **1999**, *9*, 105−111.

(5) (a) Kepert, C. J.; Rosseinsky, M. J. *Chem. Commun.* **1999**, 375. (b) Venkataraman, D.; Gardner, G. B.; Lee, S.; Moore, J. S. *J. Am. Chem. Soc.* **1995**, *117*, 11600−11601. (c) Li, H.; Eddaoudi, M.; O'Keeffe, M.; Yaghi, O. M. *Nature* **1999**, *402*, 276−279.

(6) (a) Baiker, A. *Curr. Opin. Solid State Sci.* **1998**, *3*, 86. (b) Akporiaye, D. E. *J. Chem. Soc., Chem. Commun.* **1994**, 1711. (c) Davis, M. E.; Lobo R. F. *Chem. Mater.* **1992**, *4*, 756.

(7) (a) Feast, S.; Bethell, D.; Page, P. C. B.; King, F.; Rochester, C. H.; Siddiqui, M. R. H.; Willock, D. J.; Hutchings, G. J. *J. Chem. Soc., Chem. Commun.* **1995**, 2409−2411. (b) Ogunwumi, S. B.; Bein, T. *Chem. Commun.* **1997**, 901. (c) Johnson, B. F. G.; Raynor, S. A.; Shephard, D. S.; Maschmeyer, T.; Thomas, J. M.; Sankar, G.; Bromley, S.; Oldroyd, R.; Gladden, L.; Mantle, M. D. *Chem. Commun.* **1999**, 1167−1168.

(8) Newsam, J. M.; Treacy, M. M. J.; Koetsier, W. T.; de Gruyter, C. B. *Proc. R. Soc. London, Ser. A* **1988**, *420*, 375.

(9) Anderson, M. W.; Terasaki, O.; Ohsuna, T.; Philippou, A.; MacKay, S. P.; Ferreira, A.; Rocha, J.; Lidin, S. *Nature* **1994**, *367*, 347−351.

10.1021/ja993814s CCC: $19.00 © 2000 American Chemical Society
Published on Web 05/16/2000

phates,[10,11] the aluminophosphates $Co(tn)_3 \cdot [Al_3P_4O_{16}] \cdot 2H_2O$ (GTex-2)[12] and *trans*-$Co(dien)_2 \cdot Al_3P_4O_{16} \cdot 3H_2O$ (GTex-3),[13] and the tin(II) phosphate $[CN_3H_6][Sn_4P_3O_{12}]$ (GUAN-SnPO).[14] The gallophosphate *d*-$Co(en)_3 \cdot [H_3Ga_2P_4O_{16}]$[15] and aluminophosphate *d*-$Co(en)_3 \cdot [Al_2P_4O_{16}] \cdot 3H_2O$[16] were grown in enantiomerically pure form using a resolved template; however, all these examples collapse irreversibly upon calcination. A series of chiral but dense cobalt phosphates $XCoPO_4$ (X = NH_4, Na, K, Rb) have been reported recently.[17] Atom site ordering leads to chirality in the porous gallium germanate $(KGaGeO_4)_6 \cdot 7H_2O$ (UCSB-7K).[18] Chiral templation of zincophosphate growth has recently resulted in two mesoporous phases of unknown structure.[19] Of particular note in the quest for organic-based chiral frameworks has been the recent observation of porosity in cross-linked protein crystals.[20] The molecular frameworks Cd(tcm)[B(OMe)$_4$]·*x*MeOH,[21] Ni(tpt)$(NO_3)_2$,[22] [{Ni(bpy)(Ar-COO)$_2$(MeOH)$_2$}$_n$],[23] [{Zn(sala)$(H_2O)_2$}$_2$]·$2H_2O$,[24] Zn_2(btc)-$(NO_3) \cdot H_2O \cdot 5EtOH$,[25] and Ag(hat)$ClO_4 \cdot 3CH_3NO_2$[26] are all chiral, the last two displaying the helical (10,3)-a network[27] and retaining crystallinity on solvent removal. A high degree of robustness to solvent removal has been reported recently in coordination frameworks incorporating chirally functionalized ligands.[28]

In this paper the combination of alcohol and pyridine equatorial ligands at an octahedral metal center connecting two trans diaxial btc ligands is shown to be a flexible recipe to prepare a wide range of chiral porous solids with large extraframework void regions. The neutral $M_3(btc)_2$ framework adopts the (10,3)-a network (also known as Y*, $SrSi_2$, or "Laves Graph", one of the seven networks of equivalent three-connected points that repeat regularly in space and have the property that the shortest circuit from any point and including *any two* of the links meeting at the point is a decagon).[27] The extent of network interpenetration is controlled by whether the alcohol ligands bound equatorially to the metal are uni- or bidentate. This network is intrinsically chiral due to the helices from which it is constructed, making the large void volume of this structure of particular interest.

Bulk homochiral samples of enantiopure networks can be prepared from resolved template molecules with the hand of the helix directly controlled by that of the diol bound to the metal. Careful desolvation below 145 °C affords crystalline samples with both empty chiral pores and vacant coordination sites around the metal centers.

Experimental Section

Synthesis: Ethylene Glycol (1,2-Ethanediol), Methanol, Ethanol, and 1-Propanol Frameworks. Single crystals of phase **A** (ethylene glycol) and phase $\mathbf{A_1}$ (other alcohols) were grown by slow diffusion of pyridine into a stoichiometric 2:3 solution of H_3(btc) (trimesic acid) and $M(NO_3)_2 \cdot 6H_2O$ (M = Ni, Co) in the desired alcohol. Three milliliters of this mixture (0.1 mmol of H_3(btc), 0.15 mmol of $Ni(NO_3)_2 \cdot 6H_2O$) was placed in one arm of the H-cell (height 90 mm, crossbar 60 mm, circular section diameter 15 mm) and in the other 0.6 mL (7.42 mmol) of pyridine. Pure solvent was carefully layered on to each side until the crossbar was full. The cell was then stoppered and left to stand. Crystals of up to 100 mm^3 were grown over a 1 month period.

1,2-Propanediol (1,2-pd), 2,3-Butanediol (2,3-bd), 1,2-Butanediol (1,2-bd), 1,2,4-Butanetriol, 1,2-Pentanediol, and 3-Chloro-1,2-propanediol. Diffusion of pyridine vapor into a stoichiometric 2:3 solution of H_3(btc) and $Ni(NO_3)_2 \cdot 6H_2O$ in the desired diol/triol yielded octahedral single crystals of phase **B** up to 1 mm in length within 2 weeks. Two milliliters of alcoholic solutions containing 10 μmol of H_3(btc) and 15 μmol of $Ni(NO_3)_2 \cdot 6H_2O$ were placed in cylindrical specimen jars, dimensions 75 × 25 mm. Approximately 0.2 mL (2.47 mmol) of pyridine was placed in a stoppered vial. The vial was placed inside the jar and its stopper pierced with a single pin prick. The jar was then sealed and left to stand.

The different methods for growing crystals of phases **A** and **B** are entirely complementary. Either method may be used to produce crystals of each phase.

Structure Determination. Single-crystal X-ray diffraction data were recorded on an Enraf-Nonius DIP2000 image plate diffractometer with Mo Kα radiation at 150 K. Crystals were quench-cooled in the nitrogen gas cryostream. In the case of the ethylene glycol salt, 90 images were recorded with successive 2° rotations in ϕ and reduced with the HKL suite of programs.[29] The 293 K structure of this phase was refined against Cu Kα radiation data obtained on an Enraf-Nonius MACH3 four circle diffractometer. Structure solution of the ethylene glycol and methanol salts (phases **A** and $\mathbf{A_1}$, respectively) was by a combination of geometric considerations and Fourier techniques using SHELXL-93.[30] Structures of the 1,2-propanediol and 2,3-butanediol salts (phase **B**) were solved using Patterson methods in SHELXS-86[31] and subsequent Fourier syntheses within SHELXL-93.[30] Details of crystallographic work are given in Table 1 and the accompanying CIF files. Two separate crystals of the 1,2-propanediol phase **B** were examined and gave identical results.

Thermogravimetric analyses were performed on a Rheometric Scientific STA 1500 instrument to study the loss of encapsulated solvent as a function of time and temperature. Samples were heated under flowing nitrogen to 600 °C ramped at 2 °C min^{-1}. An atmosphere of laboratory air was used for samples heated at 40 °C for periods greater than 6 h.

Powder X-ray Diffraction Study of Sorption and Desorption. Data were recorded on a Siemens D5000 diffractometer operating in transmission geometry with capillary samples, Cu $K\alpha_1$ radiation from a Ge monochromator, and a 6° linear position sensitive detector.

(10) (a) Rajic, N.; Logar, N. Z.; Kaucic, V. *Zeolites* **1995**, *15*, 672−678. (b) Harrison, W. T. A.; Gier, T. E.; Stucky, G. D.; Broach, R. W.; Bedard, R. A. *Chem. Mater.* **1996**, *8*, 145−151.

(11) Neeraj, S.; Natarajan, S.; Rao, C. N. R. *Chem. Commun.* **1999**, 165.

(12) Bruce, D. A.; Wilkinson, A. P.; White, M. G.; Bertrand, J. A. *J. Chem. Soc., Chem. Commun.* **1995**, 2059−2060.

(13) Bruce, D. A.; Wilkinson, A. P.; White, M. G.; Bertrand, J. A. *J. Solid State Chem.* **1996**, *125*, 228.

(14) Ayyappan, S.; Bu, X.; Cheetham, A. K.; Rao, C. N. R. *Chem. Mater.* **1998**, *10*, 3308.

(15) Stalder, S. M.; Wilkinson, A. P. *Chem. Mater.* **1997**, *9*, 2168−2173.

(16) Gray, M. J.; Jasper, J. D.; Wilkinson, A. P.; Hanson, J. C. *Chem. Mater.* **1997**, *9*, 976.

(17) Feng, P. Y.; Bu, X. H.; Tolbert, S. H.; Stucky, G. D. *J. Am. Chem. Soc.* **1997**, *119*, 2497−2504.

(18) Gier, T. E.; Bu, X.; Feng, P.; Stucky, G. D. *Nature* **1998**, *395*, 154.

(19) Nenoff, T. M.; Thoma, S. G.; Provencio, P.; Maxwell, R. S. *Chem. Mater.* **1998**, *10*, 3077−3080.

(20) Vilenchik, L. Z.; Griffith, J. P.; St Clair, N.; Navia, M. A.; Margolin, A. L. *J. Am. Chem. Soc.* **1998**, *120*, 4290−4294.

(21) Batten, S. R.; Hoskins, B. F.; Robson, R. *Angew. Chem., Int. Ed. Engl.* **1997**, *36*, 636−637.

(22) Abrahams, B. F.; Batten, S. R.; Granna, M. J.; Hamit, H.; Hoskins, B. F.; Robson, R. *Angew. Chem., Int. Ed. Engl.* **1999**, *38*, 1475−1477.

(23) Biradha, K.; Seward, C.; Zaworotko, M. J. *Angew. Chem., Int. Ed. Engl.* **1999**, *38*, 492−495.

(24) (a) Ranford, J. D.; Vittal, J. J.; Wu, D. *Angew. Chem., Int. Ed. Engl.* **1998**, *37*, 1114. (b) Zaworotko, M. J. *Angew. Chem., Int. Ed. Engl.* **1998**, *37*, 1211.

(25) Yaghi, O. M.; Davis, C. E.; Li, G. M.; Li, H. L. *J. Am. Chem. Soc.* **1997**, *119*, 2861−2868.

(26) Abrahams, B. F.; Jackson, P. A.; Robson, R. *Angew. Chem., Int. Ed. Engl.* **1999**, *37*, 2656.

(27) (a) Wells, A. F. *Three-Dimensional Nets and Polyhedra*; Wiley-Interscience: New York, 1977. (b) O'Keeffe, M.; Hyde, B. G. *Crystal Structures. 1. Patterns and Symmetry*; American Mineralogical Society Monograph, 1996.

(28) Kiang, Y.-H.; Gardner, G. B.; Lee, S.; Xu, Z.; Lobkovsky, E. B. *J. Am. Chem. Soc.* **1999**, *121*, 8204.

(29) Otwinowski, Z.; Minor, W. *Processing of X-ray Diffraction Data Collected in Oscillation Mode*; Otwinowski, Z., Minor, W., Eds.; Academic Press: New York, 1996; p 276.

(30) Sheldrick, G. M. *SHELXL-93 Program for the refinement of crystal structures*; Universität Gottingen, 1993.

(31) Sheldrick, G. M. *SHELXS-86*; Universität Gottingen, 1986.

Table 1. Crystal Data and Refinement Summaries for All Structures Discussed

	solvent: ethylene glycol[32] phase: A (4 × (10,3)-a)		solvent: 1,2-propanediol phase: B (2 × (10,3)-a′)	solvent: 2,3-butanediol phase: B (2 × (10,3)-a′)
formula	$C_{66}H_{98}N_6O_{34}Ni_3$	$C_{66}H_{98}N_6O_{34}Ni_3$	$C_{81}H_{124}N_6O_{34}Ni_3$	$C_{84}H_{126}N_6O_{30}Ni_3$
FW/g mol^{-1}	1695.63	1695.63	1901.99	1876.04
T/K	150(2)	293(2)	150(2)	150(2)
λ/Å	0.71073	1.54180	0.71073	0.71073
description	blue octahedra	blue octahedra	blue octahedra	blue octahedra
size/mm^3	0.40 × 0.375 × 0.35	0.40 × 0.375 × 0.35	0.22 × 0.22 × 0.22	0.15 × 0.15 × 0.15
crystal system	Cubic	Cubic	cubic	cubic
space group	$P4_232$	$P4_232$	$I4_132$	$I4_132$
a/Å	15.922(1)	16.025(1)	28.471(1)	28.457(1)
V/Å^3	4036.4(4)	4115.2(4)	23078.5(14)	23044.5(14)
Z	2	2	8	8
ρ_{calc}/Mg m^{-3}	1.395	1.368	1.095	1.081
μ/mm^{-1}	0.781	1.538	0.553	0.550
$2\theta_{max}$/deg	53.46	149.38	52.82	45.28
data/restraints/parameters	1445/37/124	1347/37/124	3947/10/147	2562/44/114
$R(F)$/% {$I > 2\sigma(I)$, all data}	0.0965, 0.1233	0.0697, 0.0945	0.0817, 0.1266	0.1719, 0.1740
$R_w(F^2)$/% {$I > 2\sigma(I)$, all data}	0.2426, 0.2599	0.1889, 0.2046	0.2072, 0.2366	0.4277, 0.4291
GOF	1.220	1.056	0.951	1.384
Flack parameter	0.03(11)	−0.04(15)	−0.02(4)	0.13(11)

Resolvation was studied by allowing open capillaries to equilibrate with solvent vapor in closed containers. Resolvation, as seen by changes to the XRD pattern, is not seen to occur when samples are left to stand in air, ruling out the possibility that water is responsible for the resolvation behaviors observed.

Vibrational Spectroscopy. Infrared data were collected on samples prepared as KBr disks in airtight cells over the range 400 to 4000 cm^{-1} using a Mattson Instruments Galaxy Series FTIR 6020 spectrometer. Raman data were collected with a Dilor Labram14/23IM spectrometer using a 20 mW HeNe laser (632 nm) and the sample placed on a clean microscope slide in air.

Gas Chromatography. Single crystals of phase **B** were removed from the vessel in which they were grown from racemic 1,2-propanediol and dried on filter paper. Individual crystals (ca. 1.5 mg, 0.7 μmol) were dissolved in a minimum volume, ca. 2 mL (35 mmol), of glacial acetic acid and the resulting solution diluted 100 times by ethyl acetate. For each crystal five 2 μL portions of this solution were injected into a SUPELCO α-DEX 120 GC column held at a steady 80 °C. Detection of eluted components was carried out by a Fisons GC8000 series gas chromatogram. An 80 °C isotherm and a helium carrier pressure of 100 kPa gave near baseline resolution of (*R*)- and (*S*)-1,2-propanediol. This experiment was repeated on three different crystals.

Solution NMR. Solid samples (ca. 5 mg) were dried briefly on filter paper and dissolved in the minimum volume of dilute HNO_3 in D_2O. Solution ^{1}H NMR spectra in D_2O were recorded on a Varian Mercury 300 MHz spectrometer.

Results

The diffusion crystal growth outlined above produces three new but related structural families. The ethylene glycol (**A**) and methanol/ethanol/1-propanol (**A$_1$**) structures contain four interpenetrating (10,3)-a networks with cubic and tetragonal crystal symmetry, respectively, while the 1,2-propanediol family have a much more open structure with only two interpenetrating, distorted networks. The structure of the tetragonal phase **A$_1$** is massively disordered and will be described in detail in a separate publication. The yields are difficult to determine precisely due to wetting of the product by the solvent, but are typically of the order of 75% based on the metal.

Fourfold Interpenetration of the (10,3)-a Net in A (Ethylene Glycol). $Ni_3(btc)_2(py)_6(eg)_6\cdot(eg)_x\cdot(H_2O)_y$ ($x \approx 3$, $y \approx 4$) and an analogous Co^{II} phase grow as octahedral blue and red crystals, respectively, both of which are insoluble in water and common organic solvents. The systematic absences (*00l*: $l = 2n + 1$), $m\bar{3}m$ Laue symmetry, and structural modelings defined the space group as $P4_232$ (No. 208), making these the first molecular materials to crystallize with this symmetry. A brief description of this phase has been given in a previous communication.[32] Here we concentrate on demonstrating how the pores form around the templating unit, and how these pores are linked into channels despite the network interpenetration. The tridentate btc anions are connected linearly by the Ni^{II} cations. The two btc ligands per metal occupy axial positions trans to each other in the octahedral coordination sphere of Ni^{II}, with the equatorial positions being occupied in a disordered manner by 50% ethylene glycol and 50% pyridine. (Figure 1a). The trans btc groups are orientated approximately orthogonal to each other due to a hydrogen bonding interaction between the noncoordinated oxygen atom of the btc carbonyl group and the equatorial alcohol group (O11···O2 = 2.60 Å), as shown in Figure 1a: the alcohol ligands are locally cis, generating the perpendicular arrangement of the btc planes. This interaction thus generates the three-dimensional (10,3)-a rather than a planar (6,3) network structure.

Framework Structure of A. Four equivalent (10,3)-a networks, each related by unit translation or 2-fold rotation, interpenetrate in a manner foreseen by Wells[27a] but are seen here chemically, we believe, for the first time (Figure 1b). The four btc anions per unit cell define a body-centered cubic array of pseudotetrahedral cavities, centered on the 2*a* 0,0,0 and $^1/_2,^1/_2,^1/_2$ special positions, which are linked by channels running parallel and diagonal to the unit cell edges (Figure 2a,b). The pores occupy 28% of the crystal volume, as calculated by summing voxels more than 1.2 Å away from the van der Waals surface of the framework.[33] Each has a volume of ca. 600 Å^3 and a maximum diameter of 12 Å (calculated using VDW radii). The highly diffuse electron density in the pores was modeled as arising from a 3-fold disordered, pseudotetrahedral cluster of four ethylene glycol molecules linked together by hydrogen bonding (denoted by a network of 2.80 Å intermolecular O···O distances), which is illustrated in Figure 2c. Each eg is located over the centroid of a btc unit from each of the four (10,3)-a nets and thus this $(eg)_4$ supramolecular assembly templates the quadruply interpenetrating network structure.

The (10,3)-a network is inherently chiral due to the ⟨100⟩ 4-fold (e.g., 4_2 helices parallel to the cubic cell vectors in Figure 1b) and ⟨111⟩ 3-fold helices. The four sets of helices in **A** have

(32) Kepert, C. J.; Rosseinsky, M. J. *Chem. Commun.* **1998**, 31−32.
(33) Spek, A. L. *Acta Crystallogr., Sect. A* **1990**, *46*, C34.

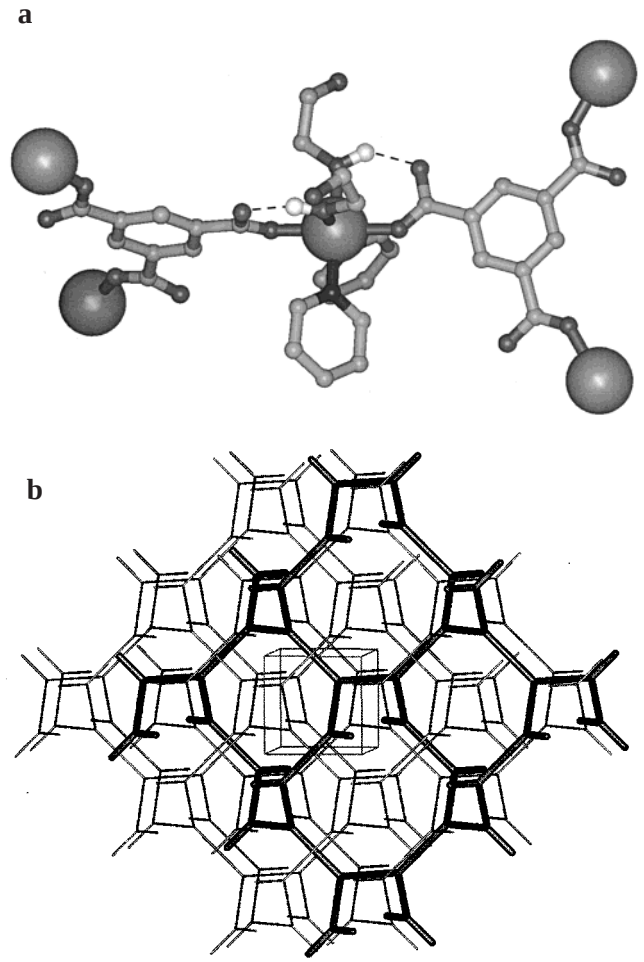

Figure 1. (a) Coordination at the nickel cation in **A**. The axial positions are occupied by two *trans*-1,3,5-benzenetricarboxylate (btc) ligands which each coordinate to three nickel cations. The orientations of these btc units are controlled by hydrogen bonding (dashed lines) to the two cis unidentate ethylene glycol (eg) molecules. The coordination is completed by two pyridine molecules. (b) Quadruple interpenetration of the (10,3)-a net (denoted 4 × (10,3)-a) in **A**: 3-fold sites (representing btc) are linked together by linear rods (representing nickel). One of the four equivalent nets has been highlighted for clarity.

the same handedness and the refined value of the Flack parameter (0.03(11)) shows that each crystal of the chiral framework phase grows as one single enantiomer, with homochiral pores and channels. This spontaneous resolution originates in the inability of helices of opposite handedness to intergrow due to the inter-btc repeat. As no part of the initial reaction mixture is intrinsically chiral, bulk samples will be 50:50 mixtures of left- and right-handed helical crystals.

Twofold Interpenetration of a Distorted (10,3)-a Net in B (1,2-Propanediol and 2,3-Butanediol). The search for a suitable template to grow homochiral bulk samples of **A** led to the use of the methyl-substituted chiral glycol 1,2-propanediol (1,2-pd) as solvent. This apparently insignificant change leads to the synthesis of a yet more expanded chiral phase, **B**, derived from a network that is a pronounced distortion of the aristotype (10,3)-a net. The distortion arises from the intercentroid vectors no longer being coplanar, with the angles between the inter-btc vectors changing from 120° in (10,3)-a to 114.27° in phase **B**. Phase **B**, which is insoluble in water and common organic solvents, is shown for the 1,2-pd solvate to have the composition $Ni_3(btc)_2(py)_6(1,2\text{-pd})_3 \cdot 11(1,2\text{-pd}) \cdot 8(H_2O)$ by chemical analysis (calcd: C 47.52, H 7.28, N 3.69, Ni 7.74. Found for two distinct samples: C 47.49, H 6.31, N 3.67, Ni 7.76, and C 47.56, H

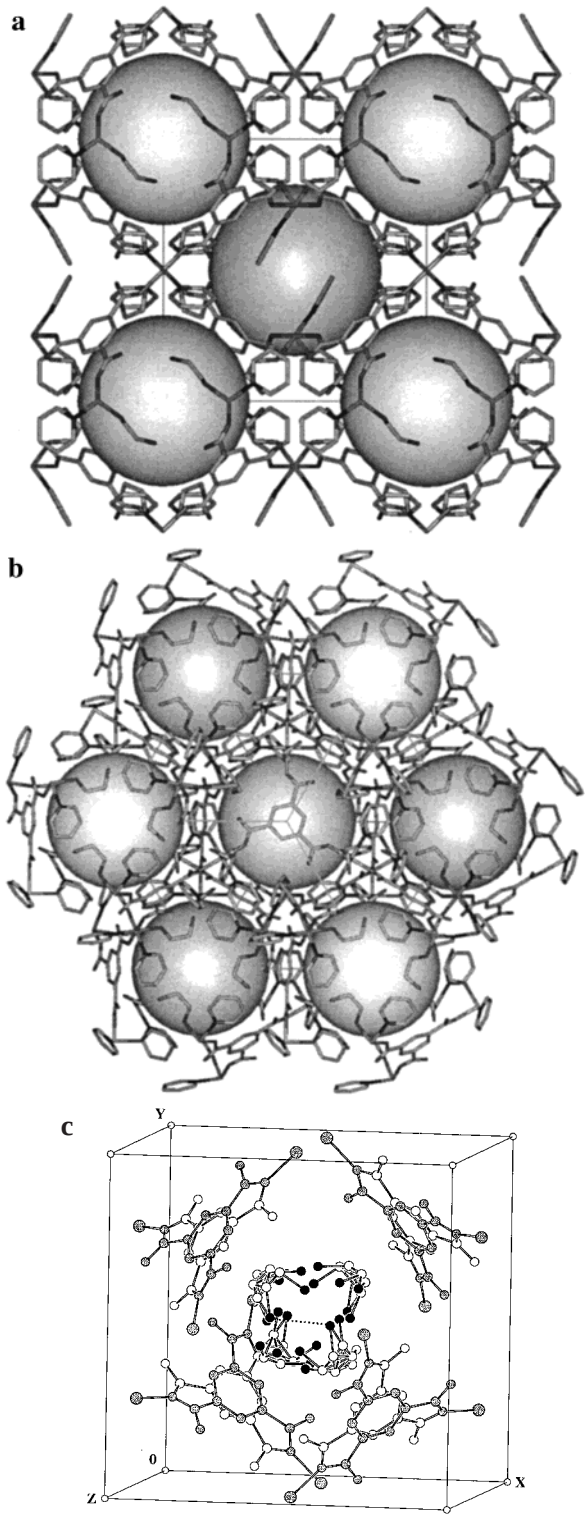

Figure 2. (a) Structure of **A** viewed along the [100] direction. Cavity centers are marked with large spheres and are occupied by the units displayed in panel c. The channels between the cavities along this direction link next-nearest neighbor cavities separated by *a*. (b) Structure of **A** viewed along the [111] direction showing the pseudohexagonal channels defined by pyridine and ethylene glycol ligands. (c) The highly disordered, hydrogen bonded $(eg)_4$ cluster at the cavity center in **A**. Oxygen atoms in this cluster are shaded black. Atoms shaded gray show the two orientations of the btc units, whose disorder is coupled with that of the equatorial pyridine and ethylene glycol ligands. Each eg is located over the centroid of a btc from each of the four (10,3)-a networks, producing a templating effect. The closest C···C contacts of 3.73 Å are between the eg and btc benzene ring carbon atoms.

7.43, N 3.65, Ni 7.72) This phase adopts the space group $I4_132$ (No. 214), determined unambiguously from the systematic absences and also unique for a molecular material. Both structures are highly disordered, with the equatorial ligands and nickel atoms in the framework disordered onto two sites. We will focus our discussions on the 1,2-propanediol solvate, for which a greater degree of structural information was obtained, due to the increased framework disorder in the 2,3-butanediol solvate.

The low density of the new structure **B** arises because only two distorted (10,3)-a nets interpenetrate, related by the body-centring translation (Figure 3a). This arrangement, where both networks are of the same handedness, is also new to chemistry and appears not to have been foreseen (whereas two oppositely handed regular (10,3)-a networks are known to interpenetrate highly efficiently).[34] The origin of the distortion away from the regular (10,3)-a net is in the fundamental modification of the binding of the vicinal diol to the metal, as the 1,2-propanediol molecule is now bidentate and occupies two adjacent equatorial positions at the metal (Figure 3b). The other two cis equatorial positions are occupied by symmetry-equivalent pyridine molecules. The framework is again generated using octahedral Ni as a linear connector, with the trans diaxial positions occupied by two tridentate btc ligands.

The refinement (absolute structure parameter for two separate crystals −0.02(4) and 0.00(5)) indicates that each crystal again grows from racemic 1,2-propanediol as a single enantiomer, but in this case a novel templating effect is revealed due to the chirality of the equatorial diol. Refinement clearly shows that in the crystals examined only the *S* enantiomer of the diol ((*S*)-1,2-pd) is bound to the metal, demonstrating that the anticlockwise screw chirality of the 4_3 helices can be directly controlled by the stereochemistry of the equatorial ligands (see Figure S1 in Supporting Information for an ORTEP diagram). This observation has been confirmed in two separate structure refinements on different 1,2-pd-templated crystals, and the same effect is evident in the structure of the 2,3-butanediol analogue. The direct relationship between the hand of the diol bound to the metal and that of the resulting helical nets is thus unambiguously demonstrated.

The diol bound to the metal now makes two hydrogen bonds to the btc ligands via each hydroxyl group (O2···O11 = 2.62 Å: Figure 3b). This produces a distortion of the (10,3)-a network away from the ideal geometry (where the torsion angle between adjacent btc planes is the tetrahedral angle) found in the ethylene glycol salt, since the Ni^{II} centers lie displaced out of the planes of the btc units. A similar cubic distortion of the (10,3)-a network is seen in nonporous transition metal oxalate frameworks.[35] The total pore volume calculated by summing voxels more than 1.2 Å away from the van der Waals surface of the framework[33] is 51% of the total crystal volume. Table 2 shows a range of diols and triols which give rise to this structure, and the unit cell parameters and volumes.

Similarly to **A**, it is possible to locate solvent molecules in the extraframework space but their stereochemistry, unlike that of the diol bound directly to the metal, cannot be defined crystallographically. One 1,2-pd molecule is heavily disordered about the $8a$ $^1/_8,^1/_8,^1/_8$ positions: the disorder is too extensive to permit location of the methyl group. The other pore solvent molecule is located by hydrogen bonding to the carbonyl oxygen atom of the btc ligand (Figure 3c). The data do not allow a full refinement of a model containing both enantiomers at this site: the model presented in the accompanying CIF file uses only the hand of the guest (*S*, i.e., equivalent to that of the diol directly bound to the metal) which is favored by refinement, although a highly constrained competitive refinement indicates a 68:32 ratio of (*S*)- and (*R*)-1,2-pd at this position.

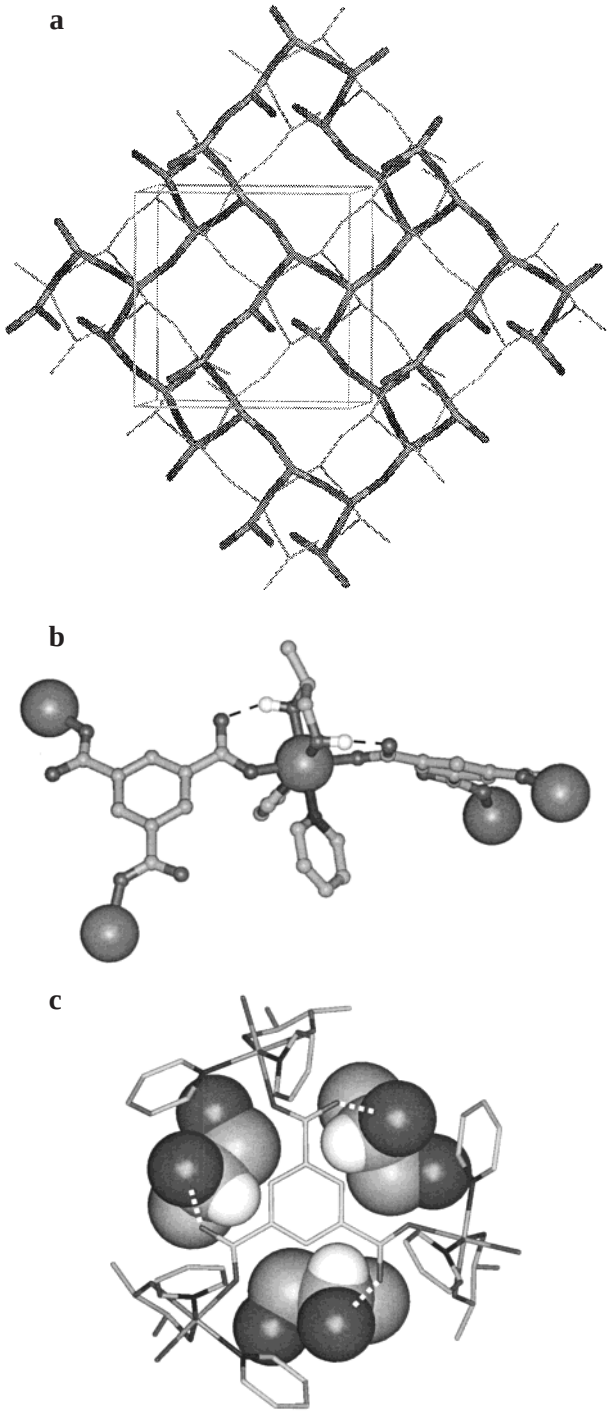

Figure 3. (a) Double interpenetration of the (10,3)-a′ net in **B** (denoted 2 × (10,3)-a′). These nets, one of which has been highlighted for clarity, are distorted substantially from the regular (10,3)-a network as seen in **A**. (b) The coordination environment at the metal center in **B** differs from that in **A**, with the diol, in this case 1,2-propanediol, now bidentate. The hand of the diol bound to the metal controls that of the helices within the (10,3)-a′ network. (c) Of the noncoordinating 1,2-propanediol (1,2-pd) molecules occupying the chiral cavities of **B**, those located closest to the (10,3)-a′ nets are located by hydrogen bonding to the carbonyl group of the btc anion. Refinement indicates that this position is preferentially occupied by the (*S*)-1,2-pd enantiomer.

(34) (a) Luzzati, V.; Spegt, P. A. *Nature* **1967**, *215*, 701−704. (b) Hyde, S. *Forma* **1998**, *13*, 145−178.

(35) Decurtins, S.; Schmalle, H. W.; Schneuwly, P.; Ensling, J.; Gütlich, P. *J. Am. Chem. Soc.* **1994**, *116*, 9521−9528.

Table 2. Summary of Crystal Data for Phases A (4 × (10,3)-a) and B (2 × (10,3)-a′)

metal	alcohol	framework	space group	*A*/Å	*c*/Å	*V*/Å^3	*T*/K
Ni	ethylene glycol	4 × (10,3)-a	$P4_232$	15.922(1)		4036	150(2)
				16.025(1)		4115	295(2)
Co	ethylene glycol	4 × (10,3)-a	$P4_232$	16.009(5)		4103	150(2)
Ni	Methanol	4 × (10,3)-a	$P4_122/P4_322$	16.292(1)	29.139(1)	7734	150(2)
Ni	Ethanol	4 × (10,3)-a	$P4_122/P4_322$	16.282(5)	30.011(8)	8195	150(2)
Ni	1-propanol	4 × (10,3)-a	$P4_122/P4_322$	16.288(4)	30.811(10)	8174	295(2)
Ni	1,4-butanediol	4 × (10,3)-a	$P4_122/P4_322$	16.235(7)	30.329(16)	7994	295(2)
Ni	1,3-propanediol	4 × (10,3)-a	$P4_122/P4_322$	15.719(2)	33.590(6)	8300	295(2)
Ni	allyl alcohol	4 × (10,3)-a	$P4_122/P4_322$	16.212(21)	30.246(47)	7950	295(2)
Ni	1,2-propanediol	2 × (10,3)-a′	$I4_132$	28.471(1)		23079	150(2)
				28.900(6)		24186	295(2)
Ni	2,3-butanediol	2 × (10,3)-a′	$I4_132$	28.457(1)		23045	150(2)
				28.837(2)		23980	295(2)
Ni	1,2-butanediol	2 × (10,3)-a′	$I4_132$	28.988(2)		24359	295(2)
Ni	1,2-pentanediol	2 × (10,3)-a′	$I4_132$	28.970(4)		24313	295(2)
Ni	3-chloro-1,2-propanediol	2 × (10,3)-a′	$I4_132$	28.970(2)		24313	295(2)
Ni	1,2,4-butanetriol	2 × (10,3)-a′	$I4_132$	29.5(3)		25700	150(2)

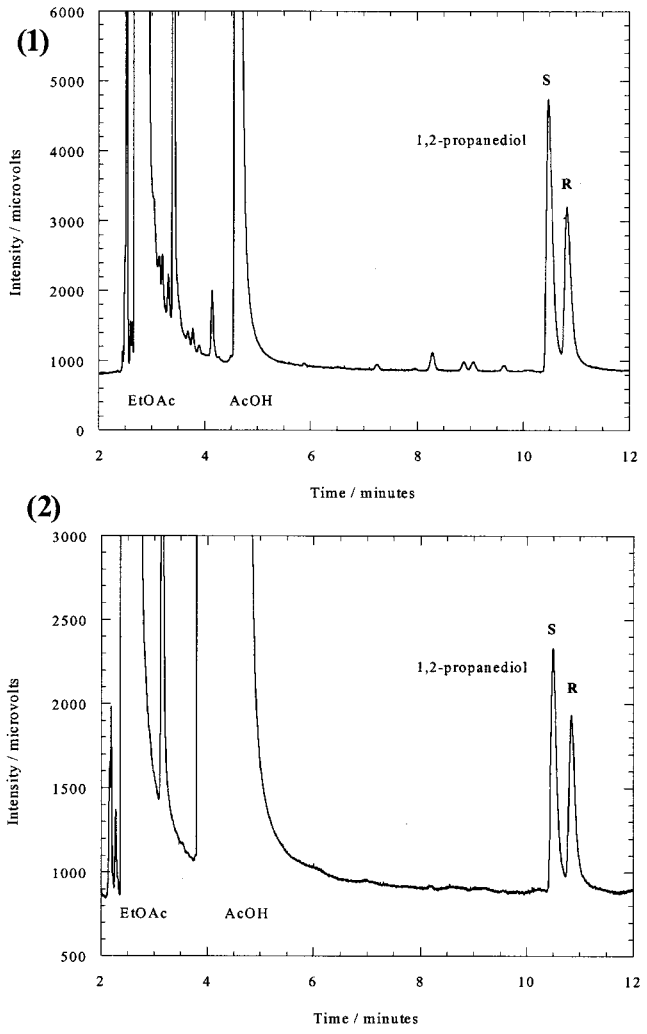

Figure 4. Gas chromatograms for 1,2-propanediol in a mixture of ethyl acetate and acetic acid solvents. (1) A sample of racemic 1,2-pd enriched with approximately 50% (*S*)-1,2-pd. The *S*:*R* ratio is 1.688:1 and the ee is 25.6%. (2) A sample from a single crystal of phase **B**. The *S*:*R* ratio is 1.46:1 and the ee is 18.7%.

Chiral GC shows that the ratio of enantiomers of 1,2-pd in a single crystal of **B** is 1.46(2):1. The crystallographic evidence suggests that the enantiomer bound to the metal is in excess (18.7% enantiomeric excess, Figure 4). The GC data are thus consistent with all of the 1,2-pd on the 8*a* positions and ca. one tenth of the 1,2-pd which hydrogen bonds to the framework having the opposite configuration to the 1,2-pd bound to the metal. It should be noted that the same structure results upon crystallization from the resolved template alcohol, removing the possibility that the phase requires racemic but disordered solvent to be present in the pores for stability.

Guest Desorption To Form Chiral Porous Phases. The thermogravimetric behavior of **A** and accompanying changes in X-ray powder diffraction patterns on thermal loss of both cavity and bound solvent are shown in Figure 5. The large weight loss between 100 and 150 °C is consistent with loss of all of the cavity solvent and 16% of the ligands bound to the metal. This corresponds to a change in composition from that of as-grown **A** shown by chemical analysis to be $Ni_3(btc)_2(py)_6(eg)_6{\cdot}3(eg){\cdot}4(H_2O)$ (Calcd: C 46.75, H 5.83, N 4.96, Ni 10.39. Found: C 46.8, H 5.76, N 4.84, Ni 10.38) to $Ni_3(btc)_2(py)_{4.6}(eg)_{5.2}$ (Calcd: C 48.34, H 4.72, N 5.05, Ni 13.78. Found: C 47.86, H 4.72, N 5.01, Ni 13.71). This corresponds to a weight loss of 24.7%, which is in reasonable agreement with the mass loss of ca. 30% observed. X-ray powder diffraction data show that this desolvated phase is highly crystalline, retaining the chiral 4 × (10,3)-a structure of **A** with an empty pore system and displaying negligible contraction of the cell dimension from 16.025(2) to 16.001(2) Å (corresponding to only a 0.45% decrease in volume). Heating to above 300 °C causes further loss of ligands bound to the metal and total loss of crystallinity.

Heating phase **B** to 150 °C at 2 °C min^{-1} under flowing nitrogen yields a very poorly crystalline phase (Figure S2a,b) with the composition obtained from chemical analysis as $Ni_3(btc)_2(py)_{2.8}(1,2\text{-pd})_{2.3}(H_2O)_2$ (Calcd: C 45.67, H 4.19, N 3.83, Ni 17.21. Found: C 45.81, H 4.79, N 3.84, Ni 17.23). Infrared measurements show that the splitting between symmetric and asymmetric carboxylate stretch frequencies (Δ) is unchanged at 185 ± 1 cm^{-1} and it therefore appears that the carboxylate coordination does not alter with degree of desolvation.[36] The value of Δ for potassium trimesate is 201 ± 1 cm^{-1}, hence the value obtained for phase **B** is consistent with the "pseudo-bridging" hydrogen bonded geometry observed in the as-grown phase.[37]

Thermogravimetric behavior for all of the (10,3)-a′ phases isostructural with **B** is shown in Figure S3 in the Supporting Information. The generation of porous chiral phases with this structure is best illustrated by the 1,2-butanediol phase (Figure 5b), which has a composition obtained from chemical analysis

(36) Nakamoto, K. *Infrared and Raman Spectra of Inorganic and Coordination Compounds Part B*, 5th ed.; Wiley: New York, 1997.
(37) Deacon, G. B.; Phillips, R. J. *Coord. Chem. Rev.* **1980**, *33*, 227−250.

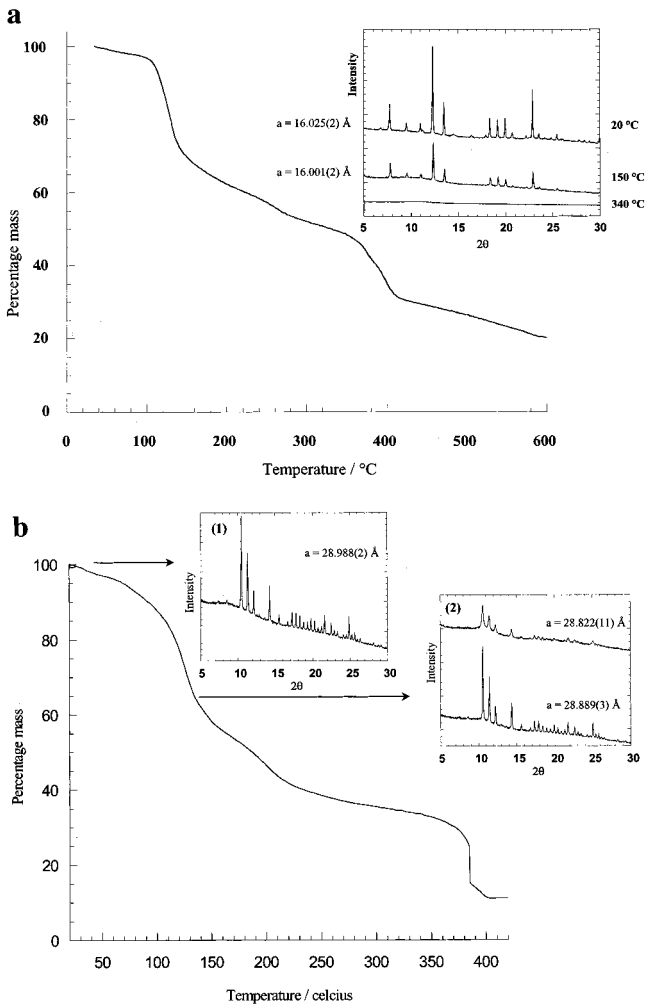

Figure 5. (a) The behavior of phase **A** (ethylene glycol analogue) upon thermal desolvation. The thermogravimetric analysis (line) and the inset X-ray powder diffraction data (collected from the TGA sample itself after runs were halted at the temperatures indicated) together show that crystalline chiral phases with vacant pores are attainable. (b) The behavior of phase **B** (1,2-butanediol analogue) upon thermal desolvation. As for phase **A**, retention of crystallinity with heating indicates the formation of a chiral microporous material supporting void volume. The upper trace in inset 2 displays the PXRD pattern showing reduction in crystallinity when the sample is held at 138 °C for 2 min.

as $Ni_3(btc)_2(py)_6(1,2\text{-}bd)_3 \cdot 10(1,2\text{-}bd) \cdot 5.5(H_2O)$ (Calcd: C 51.61, H 7.64, N 3.61, Ni 7.57. Found: C 51.60, H 7.20, N 3.38, Ni 7.55) and begins to lose cavity guest molecules rapidly at 90 °C. Inspection of thermogravimetric data for this phase reveals a point of inflection at approximately 138 °C. Heating to 138 °C at 2 °C min^{-1} in flowing nitrogen leads to a material with the composition obtained from analysis as $Ni_3(btc)_2(py)_{4.8}(1,2\text{-}bd)_{9.6}(H_2O)_4$ (Calcd: C 50.60, H 7.09, N 3.52, Ni 9.24. Found: C 50.61, H 7.14, N 3.53, Ni 9.26), which is in reasonable agreement with the observed loss of mass (Calcd: 18.4%; Found: 22.6%). This is accompanied by a reduction in the crystallinity of this phase and only a 1.0% decrease in volume with a change in the unit cell parameter from 28.988(2) to 28.889(3) Å. For the fresh material the fwhm for the (222) reflection at $2\theta = 10.51°$ is 0.1042°, compared with 0.1155° for the desolvated phase. Heating the material to 138 °C as described above and then holding at this temperature for 2 min generates $Ni_3(btc)_2(py)_{4.1}(1,2\text{-}bd)_{6.8}(H_2O)_6$ (Calcd: C 48.24, H 6.58, N 3.53, Ni 10.73. Found: C 48.25, H 6.34, N 3.49, Ni 10.70), which is in good agreement with the observed mass loss (Calcd: 29.7%; Found: 30.0%). A further reduction in the crystallinity of this material is observed as demonstrated by the fwhm of the (222) reflection at $2\theta = 10.61°$ which is 0.2636°. The unit cell parameter is now 28.822(11) Å, showing an additional ca. 1% volume contraction of the framework upon further desolvation.

Guest Resorption and Framework Interconversion. The crystallinity of **A** and **B** can be significantly degraded by ligand loss within the primary coordination sphere of the metal, when the weight loss extends beyond the first inflection points in the TGA data of Figure 5a,b. This process is not irreversible, however, and the crystallinity of the starting material can be regenerated in both cases by exposing the poorly crystalline desolvated intermediate to ethanol, methanol, or ethylene glycol vapor at room temperature. The behavior of phase **A** is summarized in Scheme 1 and Figure S4, both in the Supporting Information.

The (10,3)-a network phase generated by methanol and ethanol resolvation of **A** has cubic rather than tetragonal symmetry after 1 day of exposure, indicating that the low-temperature resorption is controlled by the nature of the cubic network remaining after desolvation of the original cubic phase **A**. This demonstrates that the local structure is retained despite the poor crystallinity. After 1 week the structure relaxes to give the tetragonal form which grows directly from solution. In contrast, desolvation of the tetragonally distorted ethanol phase $\mathbf{A_1}$ followed by resorption of ethanol from the vapor phase over a 1 week period affords the tetragonally distorted framework.

Desolvation of phase **B** (1,2-propanediol) at 40 °C for 24 h yields an amorphous phase. Resolvation of this material with ethanol vapor is shown in Figure 6a. After 30 h exposure the diffraction pattern is characteristic of the "two network" phase with $a = 28.9(1)$ Å, but displays several small features due to the "four network" phase. This contrasts with the direct growth of the "four network" phase $\mathbf{A_1}$ from ethanol and is an indicator that the cavities and channels in crystalline solvated **B** are present in the poorly crystalline desolvated material and direct the course of the resolvation: dissolution and growth would result in the $\mathbf{A_1}$ 4 × (10,3)-a structure. A further exposure to ethanol vapor for 2 days gives a pattern that is a mixture of both **A** and **B**, while after 8 days the pattern indicates complete conversion to the cubic four-network phase **A**. This is consistent with the more dense four-network phase being more thermodynamically stable than the two-network phase **B**, which forms more easily kinetically due to the retention of the characteristics of the more expanded phase in the poorly crystalline intermediate. Combined solution NMR, Raman (Figure S5, Supporting Information), and chemical analysis studies for a sample of the desolvated material placed in ethanol for a period of 5 days demonstrate the resorption of ethanol into the cavities. ^{1}H NMR shows that ca. 30 times more ethanol than 1,2-propanediol is present in the sample. This information, combined with microanalysis, suggests a composition of $Ni_3(btc)_2(py)_{5.9}(1,2\text{-}pd)_{0.35}(C_2H_5OH)_{10.9}(H_2O)_{6.5}$ (Calcd: C 49.61, H 6.92, N 4.85, Ni 10.33. Found: C 49.62, H 5.74, N 5.07, Ni 10.24). Resolvation with methanol or 2-methyl-1-butanol (Figure 6b) results in formation of the two-network phase which shows no tendency to relax to the four-network structure. This clathrate-like behavior of a poorly crystalline intermediate phase has been noted in other molecular framework systems.[25] Resolvation of phase **B** desolvated at 150 °C is dealt with in Figure S5 of the Supporting Information.

Discussion

Both phases contain the chiral, helical $M_3(btc)_2$ (10,3)-a net where the 3-connected btc units are joined by 2-fold Ni

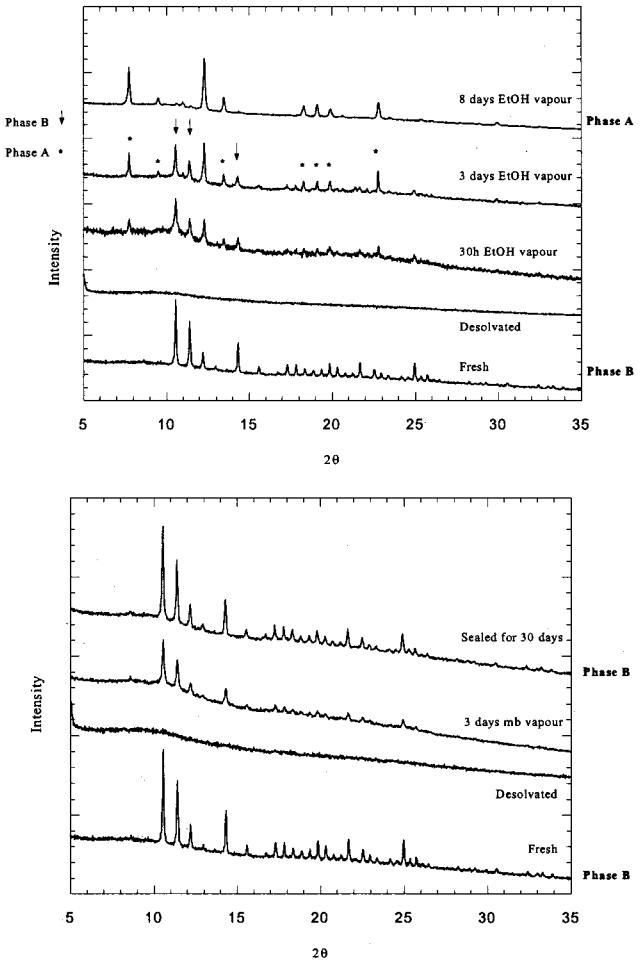

Figure 6. (a) Evolution of the X-ray diffraction pattern of phase **B** (1,2-propanediol analogue) upon desolvation and subsequent resolvation with ethanol vapor. The resolvated phase initially adopts the phase **B** structure and then transforms to the more stable phase **A** type after 8 days. After 3 days of exposure both phases are present, and their Bragg reflections are denoted separately. (b) X-ray powder diffraction shows that desolvation and resolvation of phase **B** with 2-methyl-1-butanol follows a different path, with the phase **B** structure being retained despite the observation that direct growth with 2-methyl-1-butanol gives a layered rather than a framework structure. The crystallinity of the resolvated phases is indicated by the fwhm of the 222 reflection at $2\theta = 10.54°$ is 0.1185° compared with 0.1001° in the starting material.

connectors, with quadruple interpenetration of the regular net in **A** and double interpenetration of a distorted net in **B**.

The observation of guest sorption/desorption from the interpenetrating frameworks here is of interest as it goes against the impression gleaned from the current literature that interpenetration and porosity are mutually exclusive. The reversible guest loss demonstrated for **A** below 145 °C indicates that the solvent molecules are able to diffuse through the channels of this network. The 2*a* cavities occupied by the $(eg)_4$ template unit define a bcc array, with each pore surrounded by eight neighbors. Four of these are joined by a common btc node, which clearly blocks solvent motion, but the other four near-neighbor cavities (e.g. those at the 0,0,0 and 1,1,1 positions for the $^1/_2,^1/_2,^1/_2$ site) can be accessed by passage through pseudo-hexagonal tunnels along the ⟨111⟩ directions (Figure 2b). These tunnels have a diameter of 3−7 Å depending on the local arrangement of equatorial ligands around the metal center (these channels, in contrast to the pores, are bounded by the py and eg ligands).

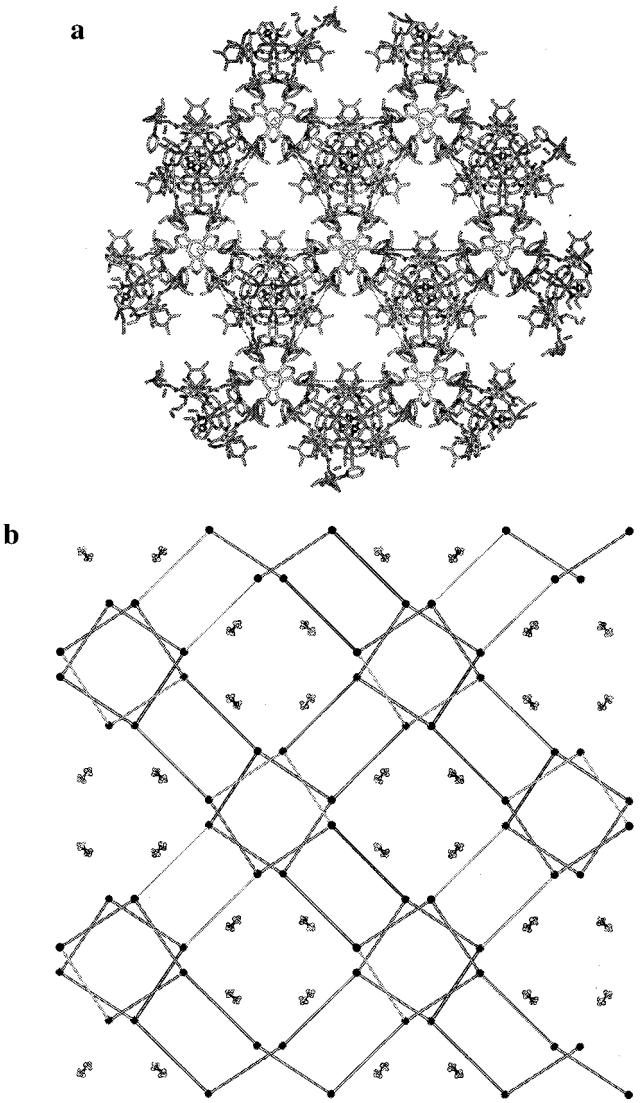

Figure 7. (a) The network structure of phase **B** viewed along [111] showing the large channels (maximum and minimum dimensions are 16.0 and 10.5 Å, respectively) running in this direction. All the framework atoms are shown. (b) Projection along [100] of the 2 × (10,3)-a′ helical networks and the 1,2-propanediol molecules disordered about the 8*a* sites at the centers of the cavity system in **B**.

The pore structure of **A** thus arises from the occupation of the 2*a* site by the $(eg)_4$ template. The 8*a* solvent-filled cavities play a similar role for phase **B**, whose structure can be generated by placing btc centroids displaced by 8.27 Å along the 3-fold axis above and below the 8*a* position (Figure S6, Supporting Information). The 8*a* cavity centers define the nodes of a regular (10,3)-a network, and thus the channel system in **B** has the (10,3)-a topology. The interpenetrating array of the two helical nets, when viewed along the [111] direction (Figure 7a), contains large channels within which the extraframework solvent is located. The channel diameter at its narrowest point is 10.5 Å (defined by van der Waals surfaces) to the 1,2-pd molecule coordinated to the metal and increases to 16 Å in regions where there is intersection of the ⟨111⟩ channels. These chiral channels are therefore comparable in size to the largest found among zeolites.[6c]

The distorted (10,3)-a net of **B** is chiral and retains the 4-fold helices parallel to ⟨100⟩ that are present in **A** (Figures 3a and 7b). The bidentate 1,2-pd molecule bound to octahedral Ni is refined as a single enantiomer, showing that the anticlockwise helix recognizes the *S* enantiomer. This directing effect of the

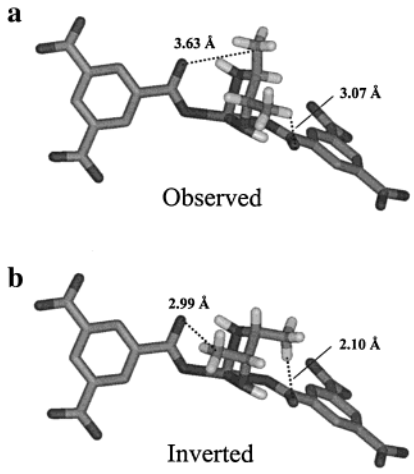

Figure 8. The origin of the chiral templating effect in phase **B**: the C···O and H···O contacts between the framework btc anion and the (*S*)-1,2-pd enantiomer bound to the metal center (as indicated by refinement) are acceptable (a), but too short if the inverted diol, (*R*)-1,2-pd, is bound in the left-handed (10,3)-a network (b). Note that the 2-fold symmetry about the metal center requires that the methyl group of the 1,2-pd has 50% occupation at two symmetry-equivalent positions, both of which are shown in each diagram.

1,2-pd ligand on the hand of the growing helix may be simply explained on the basis of the refined structure. The methyl group of the diol points away from the framework and into the helical pore structure. Inversion of the chiral center of this 1,2-pd would bring the methyl group into excessive proximity with the btc unit of the framework, which is highly unfavorable. For the observed enantiomer the closest contacts with nonbonding oxygen of the carboxylate are 3.63 (C−O) and 3.07 Å (H−O), but for the opposite enantiomer these lengths fall to 2.99 and 2.10 Å (Figure 8). This demonstrates the origin of the strong templating interaction: when the template stereochemistry is inverted, the framework−template distances are well below acceptable van der Waals radius sums of 3.22 and 2.72 Å for C···O and O···H contacts. The templating of a specific framework chirality by a particular enantiomer is thus demonstrated (both for 1,2-propanediol and 2,3-butanediol) for the first time and its origin elucidated.

In addition to the solvent at the centers of the large channels close to the 8*a* positions of $I4_132$ (Figure 7b), there are 1,2-pd molecules held by hydrogen bonding close to each node of the framework and as a result better defined crystallographically. Each of the independent (10,3)-a′ nets behaves separately in locating these 1,2-pd molecules by hydrogen bonding, with each node binding three 1,2-pd molecules (Figure 3c). In contrast with the unambiguous definition of the handedness of the diol bound to the metal, the crystallographic information on the more disordered pore solvent in both locations is not definitive. The stereochemistry of the hydrogen-bound molecule is refined as a single enantiomer, but the GC evidence indicates that the pore solvent as a whole (8*a* plus hydrogen bonded) must be nearly racemic: it is possible that this racemate is locally separated into *R* at 8*a* and *S* at the hydrogen bonded sites but better crystallographic data are required. The GC requires an *S*:*R* ratio of 1.46:1 in the crystal as a whole; this model gives a ratio of 1.8:1. However, if approximately one tenth of the (*S*)-1,2-pd located at the hydrogen-bonded sites is in fact *R*, the ratio becomes 1.5:1 and the pore solvent is approximately racemic (ee is 1.82% *R*).

The diols with terminal R rather than OH groups favor formation of the distorted (10,3)-a′ network in **B** (Table 2). These diols will hydrogen bond less effectively with cavity species than ethylene glycol due to the more hydrophobic end group, thus favoring bidentate coordination of the vicinal diol to the metal center rather than interacting with other diols in the extraframework space.

The interligand hydrogen bonding arrangements about the Ni^{II} centers in phases **A** and **B** consist of approximately planar five-membered rings. The hydrogen-bonding geometry in the two phases is remarkably similar, as shown in Figure 9a. In both cases, the alcohol ligands are cis to each other in the equatorial plane, with the btc ligands trans and diaxial. It is this cis arrangement of these hydrogen bond donors, which requires the carboxylate units of the btc molecules to be approximately perpendicular to each other, that produces the three-dimensional (10,3)-a network structure, so the use of both hydrogen bond donor and nondonor ligands in the equatorial plane is the key to the formation of these structures.

In phase **A** the angle between adjacent btc planes is the tetrahedral angle. This is possible despite the carboxylate units being perpendicular because of a rotation of ca. 9.7° along each C−C bond joining the carboxylate unit to the aromatic ring of the btc. The contraction of the ligand to metal O−Ni−O bond angle, denoted θ in Figure 9b, from a mean of 90° in phase **A** to 81.8° in phase **B** is a consequence of the geometry of the bidentate 1,2-pd molecule bound to nickel, which forms part of a five-membered ring. This in turn reduces the angle between carboxylate units from 90°. To produce an undistorted (10,3)-a network the necessary rotation about the C−C bond would be ca. 13.8°, which is not observed. The 3-fold connectivity of the network and the local coordination requirement about Ni^{II} in phase **B** are satisfied when the network contracts by approximately 10.6% in each crystallographic direction. This is accompanied by a distortion so that the centroids of adjacent btc units and the interposed nickel atom are no longer collinear, which is clearly seen in Figure 9b. The repeat length of the new network is 89.4% of that of the (10,3)-a, corresponding to a compression to 71.5% of the original network volume[38] as the nickel centers are bent rather than linear 2-fold connectors. These distortions are simply derived from the change in screw repeat from 2 × 15.9 Å to 28.5 Å, and at first sight would appear to indicate that the more compact array should produce a phase with less extraframework volume. Intriguingly, the compression of the network prevents quadruple network interpenetration and only allows two of the (10,3)-a′ nets to interpenetrate. Considerably more extraframework volume therefore results.

The two families of framework solid both have a complex desolvation/resolvation chemistry which enables, in the case of the denser phase **A**, the isolation of a phase in which analytical data indicate that all the guest species in the chiral pores have been removed. This phase is crystalline but its isolation requires careful control over the kinetics of the desolvation process. It appears to be a general feature of these phases that the desolvation processes involving loss of ligands coordinated to the metal overlap with loss of guest from the pores of the solid. This is consistent with dynamic interchange of solvent molecules between these sites in a rigid framework of metal ions defined by the Ni cations and btc anions, making it possible that desolvated crystalline **A** has empty coordination sites at the metal as well as significant voids in the channel volume. The

(38) This isotropic, cubic compression of the (10,3)-a network to the topologically identical (10,3)-a′ network supports recent predictions that 3-D helical network structures are expected to show novel mechanical properties such as negative linear and area compressibilities[39] and auxetic (negative Poisson ratio) behavior.[40]

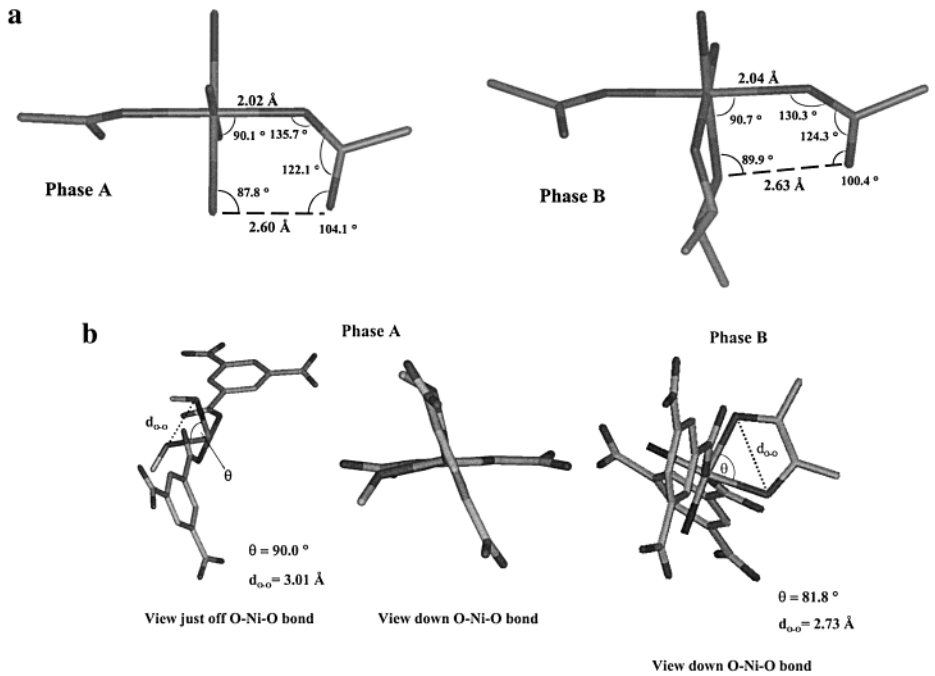

Figure 9. (a) Hydrogen bonding geometries about the metal sites in **A** and **B**. Only the O atoms of the cis ethylene glycol molecules are shown for **A**, whereas the chelating 1,2-pd molecule is shown for **B**. (b) Orientations of btc planes in **A** and **B**. The (10,3)-a net in **A** has 180° O−Ni−O angles, while the distortion in **B** yields 168.9° angles.

existence of the empty chiral pore system suggests possibilities in the area of chiral separation or induction. The extent to which this will be possible will depend on the strength of interaction between the species in the cavity and the helical (10,3)-a networks which define the chirality.

Analytical, X-ray powder diffraction and TGA measurements show that desolvated versions of both chiral frameworks can be prepared if the heating protocol is carefully controlled: once a critical fraction of the auxiliary ligands bound at the equatorial plane of the metal center are lost, the crystallinity of the desolvated phases decreases abruptly. The important question is then whether the chiral pore/channel system still survives albeit within smaller domains. Infrared spectroscopy and the results of resolvation experiments would indicate that it does. Particularly important is the outcome of resolvation of the desolvated, amorphous phase **B** with alcohols. In all cases this proceeds initially via the formation of crystalline **B** with alcohol as the guest. The combined NMR, Raman, and chemical analyses strongly suggest that the poorly crystalline intermediate contains a porous framework with open cavities that readily reabsorb alcohols. It is conceivable that upon desolvation the channels in phase **B** contract inhomogeneously, thereby reducing the crystallinity of the material, but leaving a porous structure. Upon uptake of alcohols, the channels in the structure are filled with the guest species and expand again returning the uniform dimensions of each cavity and hence the crystallinity. Since **B** forms exclusively with chelating diols, the only way it can arise with unidentate ethanol as a ligand is as the kinetic product of resolvation from the intermediate where the channels and cavities of the 2-fold interpenetrating (10,3)-a′ structure already preexist. Subsequent relaxation to the (10,3)-a structure is driven thermodynamically. It seems likely that when ethanol has diffused throughout the empty pore system it then displaces some of the 1,2-pd ligands from the metal centers. The unidentate alcohol changes the hydrogen bonding arrangement about Ni^{II}, driving the conversion to cubic phase **A**. Intriguingly, while the transformation of the distorted (10,3)-a′ network to a regular (10,3)-a requires only a geometric reorganization, the **B** to **A** transformation observed here necessitates bond breakage and reformation since it involves a modification from 2-fold to 4-fold interpenetration. Further work is underway to explore the mechanism of this transition.

2-Methyl-1-butanol, which grows directly as a hexagonal layered phase from Ni and btc with py,[41] generates the 2 × (10,3)-a′ structure on resolvation of the amorphous phase formed by heating **B** to 150°: again the preservation of the **B** structure despite the loss of crystallinity is indicated strongly by the formation of this phase by an alcohol other than a chelating diol.

Conclusions

Two families of interconvertible chiral frameworks are presented. These phases can be desolvated to yield the host structures with empty chiral pores and channels. In both cases, single crystals grown from either racemic or nonchiral alcohol templates spontaneously resolve to form homochiral helical structures featuring helical networks of uniquely one hand. **B** type frameworks form for chiral diols. This allows the specific templating of enantiopure chiral microporous phases to be demonstrated for the first time. Steric arguments clearly show that this is possible because the hand of the diol bound to the metal center dictates the chirality of the helices in the (10,3)-a net.

Combined crystallographic and GC evidence indicates that the solvent in the channels of **B** is essentially racemic, with that hydrogen bound to the btc anions being predominantly *S* (the same hand as that bound to the metal) while the solvent at the 8*a* sites and elsewhere is predominantly *R*.

The use of 3-fold connectors such as btc appears to have considerable scope in the synthesis of chiral frameworks. The

(39) Baugman, R. H.; Stafstrom, S.; Cui, C. X.; Dantas, S. O. *Science* **1998**, *279*, 1522.
(40) Evans, K. E.; Nkansah, M. A.; Hutchinson, I. J.; Rogers, S. C. *Nature* **1991**, *353*, 124.
(41) Kepert, C. J.; Prior, T. J.; Rosseinsky, M. J. *J. Solid State Chem.* In press.

demonstration that the hand of such nets can be controlled by the ligand coordinated to the metal should stimulate the search for applications of coordination polymers in enantioselective chemistry.

Acknowledgment. C.J.K. thanks Christ Church, Oxford, for a Junior Research Fellowship. We thank Professor C. K. Prout and Dr. D. J. Watkin (Chemical Crystallography Laboratory, University of Oxford) and Dr. A. Steiner and Mr. J. F. Bickley (Department of Chemistry, University of Liverpool) for access to the X-ray diffractometers (funded by UK EPSRC).

Supporting Information Available: Thermogravimetry, X-ray powder diffraction patterns, tables of bond lengths and angles (PDF) and details of crystallographic work (CIF). This information is available free of charge via the Internet at http://pubs.acs.org.

JA993814S